THE EFFECT OF SOLUTE DISSOLUTION KINETICS ON CLOUD DROPLET FORMATION

A Thesis
Presented to
The Academic Faculty
By

Akua Asa-Awuku

Masters of Science in Chemical and Biomolecular Engineering,
Georgia Institute of Technology Atlanta, GA

Spring 2006

THE EFFECT OF SOLUTE DISSOLUTION KINETICS ON CLOUD DROPLET FORMATION

Approved by:

Dr. Athanasios Nenes, ChBE and EAS
Georgia Institute of Technology

Dr. Amyn Teja, ChBE
Georgia Institute of Technology

Dr. Rodney Weber, EAS
Georgia Institute of Technology

Date Approved: January 11th , 2006

ACKNOWLEDGEMENTS

I would like to thank my advisor, Dr. Athanasios Nenes, for the countless times he has provided advice and given direction in support of my academic endeavors. Many thanks to my family whom has provided support, inspiration, and unconditional love in all my pursuits; to my friends who celebrated with me during the highs and continued to celebrate with me through the lows; and to the rest of my research group that has grown with me during this process. I have had the fortune in life to be surrounded by a network of people who have fortified my dedication to pursue my ambitions.

TABLE OF CONTENTS

LIST OF TABLES

LIST OF FIGURES

LIST OF SYMBOLS AND ABBREVIATIONS

$C_A(r,t)$ -- denotes the concentration of A [moles/m^3] at time t [sec] distance r [m] from the core droplet center

C^{eq} -- solubility in water

C^* --is the steady-state concentration of A at the droplet surface.

CCN – Cloud Condensation Nuclei

$D_{A,w}$ -- the diffusivity of A in the droplet aqueous

D_p -- the droplet diameter [m], diameter corresponding radial distance R_p

$\frac{dD_p}{dt}$ -- droplet growth rate

ΔD_p -- change is droplet diameter from droplet surface to previous droplet diameter

dr -- infinitesimal thickness, , adjacent to the droplet surface (which later on we will refer to as “surface layer”)

D_s -- diameter corresponding radial distance R_s

D_v' -- mass transfer coefficient of water vapor from the gas to the droplet.

G – growth constant parameter defined,

ΔH_v -- the latent heat of vaporization for liquid water,

$M_{w,}$ -- the molecular weight,

n_A -- moles of solute A

$\frac{dn_A}{dt}$ -- moles of A in the added condensed water vapor volume

n_s -- the moles of solute dissolved in the droplet,

k_a' -- the thermal conductivity of air

$p°(T)$ -- the vapor pressure at the ambient temperature T,

ρ_w -- density of water

r -- radial distance from core droplet center

R -- the universal gas constant

R_c, -- radial distance at the core surface,

R_s -- the distance where the dilution effect of water condensation on the droplet surface (dilution) balances diffusional supply of solute from the core

R_p --radial distance at droplet surface

s =S-1 is the supersaturation ratio

S -- ambient water vapor saturation ratio

S_c -- critical supersaturations

S_{eq} -- equilibrium saturation ratio of the growing droplet,

σ_w -- Surface tension of water,

t – time in seconds

V , droplet Volume

$\frac{dV}{dt}$, change volume of the droplet from water vapor condensation,

υ -- Van't Hoff factor,

$\omega = \frac{D_p}{D_c}$ -- ratio of particle diameter to core diameter

$\delta = 1 - \frac{D_c}{D_s}$ -- Parameterized variable.

SUMMARY

This study focuses on the importance of solute dissolution kinetics for cloud droplet formation. To comprehensively account for the kinetics, a numerical model of the process was developed. Simulations of cloud droplet growth were performed for solute diffusivity, droplet growth rates, dry particle and droplet diameters relevant for ambient conditions. Simulations suggest that high ambient supersaturations and a decrease in solute diffusivity are major contributors to significant decreases in effective solute surface concentrations. The numerical simulations were incorporated into Köhler theory to assess the impact of dissolution kinetics on the droplet equilibrium vapor pressure. For CCN composed of partially soluble material, a significant increase was found in the equilibrium supersaturation of CCN.

CHAPTER 1: INTRODUCTION

Organics constitute a major component of natural and anthropogenic particulate matter (Sloane, 1991; Wolff, 1991; Chow, 1994; Seinfeld and Pandis, 1997), yet much remains to be grasped about their effects on cloud droplet formation. Although not completely understood, carbonaceous aerosol can readily form cloud droplets (Novakov and Penner, 1993) and potentially have a strong effect on cloud formation and the hydrological cycle (Shulman et al., 1996; Facchini et al., 1999; IPCC, 2001; Feingold and Chuang, 2002; Nenes et al., 2002; Lance et al., 2004)

The theory used to describe the formation of cloud droplets from precursor aerosol, or, "cloud condensation nuclei" (CCN), was first developed by Köhler (Köhler, 1936) and has successfully been applied to CCN composed of deliquescent inorganic salt aerosols (ammonium sulfate and sodium chloride) and low molecular weight organic species that exhibit hygroscopic behavior (e.g, adipic acid and glutaric acid) (Cruz and Pandis, 1997; Raymond and Pandis, 2002). Unfortunately, the theory is less successful in describing the behavior of less hygroscopic compounds, such as those found in ambient aerosol (Cruz and Pandis, 1997; Raymond and Pandis, 2002). Analysis of ambient CCN measurements (Chuang P. Y., 2003; VanReken, 2003) typically show large deviations between predicted and measured CCN concentration under polluted conditions, which are often attributed to the complex interaction of organics with water. Organics, depending on their solubility, can contribute solute (Shulman et al., 1996; Laaksonen et al., 1998). Hydrophobic compounds with multiple functional groups may act as strong surfactants and considerably depress surface tension (Shulman et al., 1996; Facchini et al., 1999; Nenes et al., 2002); compressed surfactant layers may act as "film-forming compounds",

and may influence droplet growth kinetics enough to affect droplet number and spectral dispersion (Blanchard, 1964; Gill et al., 1983; Feingold and Chuang, 2002; Nenes et al., 2002; Chuang P. Y., 2003). Polymerization reactions, thought to occur in regions of secondary organic aerosol formation (Limbeck et al., 2003), may also have a considerable impact on the CCN properties of carbonaceous aerosol (VanReken et al., 2005). A thorough review of organics and their interactions with water vapor can be found in Kanakidou et al., 2005.

A common assumption for partially soluble compounds is that the solute instantaneously dissolves and distributes uniformly throughout the drop (Laaksonen et al., 1998; Raymond and Pandis, 2002; Shantz et al., 2003). Compared to electrolytes, the majority of organic compounds are not very soluble in water, do not deliquesce, have a higher molar mass and thus diffuse more slowly in aqueous solutions. The implication for a growing droplet is that mass transfer of the dissolving organics may not be fast enough to assure uniform distribution of solute through the droplet volume; this may decrease the solute concentration at the droplet surface and increase the droplet equilibrium vapor pressure. If sufficient, the latter may delay or even hinder droplet formation. Thus, assuming instantaneous dissolution and distribution of solute throughout the droplet volume may overestimate the effect of slightly soluble compounds on CCN activation. This kinetic limitation mechanism is fundamentally different from the growth delay identified by Shantz et al. (2003), which arises from differences in the equilibrium curves between inorganic and organic CCN.

This study focuses on exploring the effects of solute dissolution kinetics on cloud droplet formation. A numerical model is developed to simulate the dissolution of solute

from a solid core located at the center of the droplet and its diffusion throughout the aqueous phase of the growing drop. Conditions are determined for which a significant decrease in surface solute concentration is expected. The numerical simulations are parameterized and introduced into Köhler theory for a thorough analysis of dissolution kinetics on CCN behavior.

CHAPTER 2: DISSOLUTION KINETICS MODEL

2.1 Equation Formulation

The numerical model is based on the conservation of mass for the dissolving substance in a spherically symmetric droplet. The solute originates from a spherical solid core located at the center of the droplet; after dissolution, we assume that the solute mass transport occurs via molecular diffusion from the core to the droplet surface. Convective transport within the droplet phase is neglected, because i) the solution is assumed to be dilute enough so that Stefan convection is negligible, and ii) the low terminal velocity for droplets smaller than 20 μm in diameter (i.e., most CCN during their activation phase) yields negligible shear forces on their surface (Seinfeld and Pandis, 1997) hence negligible re-circulations within the droplet volume. Assuming that the solid core is composed of a slightly soluble substance A, the transport of dissolved solute from the core into the droplet aqueous phase can be described by,

$$\frac{\partial C_A(r,t)}{\partial t} = D_{Aw}\left[\frac{1}{r^2}\frac{\partial}{\partial r}\left(r^2\frac{\partial C_A(r,t)}{\partial r}\right)\right] \tag{1}$$

where $C_A(r,t)$ denotes the concentration of A at time t and distance r from the core droplet center, and D_{Aw} is the diffusivity of A in water. D_{Aw} depends on temperature and solute molecular size (Table 1).

Table 1: Aqueous diffusivity of organic compounds found in atmospheric aerosols.

Compound	Formula	$D_{A,w}$ (298 K) $m^2\ s^{-1}$	$D_{A,w}$ (273 K) $m^2\ s^{-1}$
Sodium Chloride*	NaCl	1.26×10^{-9}	
Methanol◊	CH_4O	1.94×10^{-9}	1.02×10^{-9}
Caffeine◊	$C_8H_{10}N_4O_2$	6.43×10^{-10}	3.38×10^{-10}
Adipic acid◊	$C_6H_{10}O_4$	8.19×10^{-10}	4.31×10^{-10}
Succinic acid◊	$C_4H_6O_4$	1.00×10^{-9}	5.27×10^{-10}
Suberic◊	$C_8H_{14}O_4$	7.04×10^{-10}	3.70×10^{-10}
Cholesterol◊	$C_{27}H_{46}O$	3.73×10^{-10}	1.96×10^{-10}
C_{50} (e.g, humic-like substances) ◊	$C_{50}H_{104}$	2.47×10^{-10}	1.30×10^{-10}

* obtained from (Perry et al., 1997). ◊ obtained from (Hines and Maddox, 1985).

The concentration of A throughout the droplet volume is initially equal to its solubility in water, C^{eq},

$$C_A(0, r) = C^{eq} \tag{2}$$

In terms of spatial boundary conditions, we assume that the solution is saturated with A at the core-solution interface,

$$C_A(t > 0, R_c) = C^{eq} \tag{3}$$

The boundary condition at the droplet surface is somewhat more complex, as solute diffusion and water condensation affect the surface concentration of A. $C_A(t,R_p)$ at the droplet surface can be rewritten in terms of the rate of change of freshly condensed water volume, $\frac{dV}{dt}$ and the molar flux $\frac{dn_A}{dt}$ of A into V,

$$\frac{dC_A(t,R_p)}{dt} = \frac{d}{dt}\left[\frac{n_A}{V}\right] = \frac{-n_A}{V^2}\left(\frac{dV}{dt}\right) + \frac{1}{V}\left(\frac{dn_A}{dt}\right) = \frac{-C_A}{V}\left(\frac{dV}{dt}\right) + \frac{1}{V}\left(\frac{dn_A}{dt}\right) \quad (4)$$

The freshly condensed water (hereon referred to as the "surface layer") is assumed to occupy a layer of infinitesimal thickness, *dr*, adjacent to the droplet surface. $\frac{dV}{dt}$ is equal to the rate of change of droplet volume and can be expressed in terms of the droplet diameter, D_p, as

$$\frac{dV}{dt} = \frac{\pi D_p^{\,2}}{2} \cdot \frac{dD_p}{dt} \quad (5)$$

$\frac{dn_A}{dt}$ is equal to the flux of solute from the bulk of the droplet,

$$\frac{dn_A}{dt} = -D_{Aw}\frac{\partial C_A(t,R_p - dr)}{\partial r} 4\pi (R_p - dr)^2 \approx -D_{Aw}\frac{\partial C_A(t,R_p)}{\partial r}\pi D_p^{\,2} \quad (6)$$

In equation (6), we assumed that the surface layer has negligible thickness compared to the droplet radius, so that $R_p - dr \approx R_p$. Introducing Equations (5) and (6) into (4) yields,

$$\frac{\partial C_A(t,R_p)}{\partial t} = \frac{-3}{D_p}\left[C_A\frac{dD_p}{dt} + 4D_{Aw}\frac{\partial C_A(t,R_p)}{\partial D_p}\right] \quad (7)$$

Equation (7) expresses the rate of change of C_A at the growing droplet surface and is an exact boundary condition for equation (1). $\frac{dD_p}{dt}$ can be written in terms of the ambient conditions (Seinfeld and Pandis, 1997) as,

$$\frac{dD_p}{dt} = \frac{1}{D_p}\frac{(S - S_{eq})}{G} \quad (8)$$

where $S = \frac{p^w}{p^o(T)}$ is the ambient saturation ratio, p^w is the water vapor partial pressure, $p°(T)$ is the water saturation vapor pressure at the ambient temperature T and S_{eq} is the equilibrium saturation ratio of the growing droplet. G is a kinetic growth parameter defined as $\frac{\rho_w RT}{4p°(T)D'_v M_w} + \frac{\Delta H_v \rho_w}{4k_a' T}\left(\frac{\Delta H_v M_w}{TR} - 1\right)$ where M_w and ρ_w are the molecular weight and density of water, respectively, R is the universal gas constant, ΔH_v is the latent heat of vaporization for liquid water, k_a' is the thermal conductivity of air, and D_v' is mass transfer coefficient of water vapor from the gas to the droplet. Since $S_{eq} \approx 1$ and if we neglect the size-dependence of G, Equation (8) is inversely proportional to D_p and simplifies to:

$$\frac{dD_p}{dt} \approx \frac{1}{G}\frac{S-1}{D_p} = \frac{1}{G}\frac{s}{D_p} \tag{9}$$

where $s = S - 1$ is the ambient water vapor supersaturation. Substitution of Equation (9) into Equation (7) gives,

$$\frac{\partial C_A(t, R_p)}{\partial t} = \frac{-3}{D_p}\left[\frac{1}{G}\frac{sC_A(t, R_p)}{D_p} + 4D_{Aw}\frac{\partial C_A(t, R_p)}{\partial D_p}\right] \tag{10}$$

Equation (10) is the droplet surface boundary condition used to integrate Equation (1).

2.2 Integration procedure

Equation (1), with the initial and boundary conditions expressed by Equations (2), (3) and (10) is numerically integrated using finite differences. The solution procedure

entails applying the initial condition (Equation 2) to all grid points, and then integrating the equations over time using central-differencing in the spatial direction and backward differencing in time. The boundary condition at $r = R_c$ (Equation 3) is directly applied, while the boundary condition at $r = R_p$ (Equation 10) is applied after approximating the derivatives with finite differences:

$$C_A(t+\Delta t, R_p) = C_A(t, R_p) - \frac{3\Delta t}{D_p}\left[\frac{1}{G}\frac{sC_A(t,R_p)}{D_p} + 4D_{Aw}\frac{C_A(t,R_p) - C_A(t,R_p - \Delta r)}{\Delta r}\right] \quad (11)$$

where the "new" time is "$t+\Delta t$", the "old" time is "t", and Δt, Δr are the time step and grid spacing used respectively. 5×10^4 grid points between $r = R_c$ and $r = R_p$ are used; the equations are integrated over time until steady-state is achieved.

2.3 Simulations Considered

Examination of Equation (1) and its boundary conditions (Equations 2, 3 and 10) suggests that four parameters influence the extent of surface solute concentration depression from dissolution kinetics: D_{Aw}, s, D_p and D_c. We explore the dependence of C_A to these parameters by performing a series of sensitivity simulations. To avoid any effects from transients and initial conditions, we focus on the steady-state profiles of $C_A(t,r)$; thus, to facilitate the numerical integration, we keep R_c and R_p constant during the integration.

Overall, a total of 500 simulations were completed. D_{Aw} was varied between 1×10^{-10} to 1×10^{-9} m s^{-2}, which encompasses the diversity of water-soluble organic compounds found in ambient aerosol (Table 2). Ambient supersaturations were chosen to represent globally important cloud types; we consider radiative fog (s = 0.01%),

stratiform (s = 0.25%), cumuliform (s = 0.5%) and convective clouds (s = 1%) (Pruppacher and Klett, 1997; Seinfeld and Pandis, 1997; Nenes et al., 2001). Five different droplet diameters were considered (0.1, 0.5, 1.0, 5.0 and 10 μm) to represent the transition from deliquesced aerosol to activated cloud droplets (Seinfeld and Pandis, 1997). The slightly soluble core size was also varied, expressed as a fraction of the wet diameter (0.5%, 1%, 5%, 10% and 20% of D_p).

Table 2: Parameters varied in numerical simulations.

$D_{A,w}$ (m^2 s^{-1})	*s (%)* (Cloud type)	Drop Diameter (m)	$\frac{D_c}{D_p}$
1×10^{-10}	0	0.1×10^{-6}	0.005
2.5×10^{-10}	0.01 (fog)	0.5×10^{-6}	0.01
5×10^{-10}	0.25 (stratiform)	1.0×10^{-6}	0.05
1×10^{-9}	0.5 (cumulus)	5.0×10^{-6}	0.1
	1 (cumulus)	10.0×10^{-6}	0.2

2.4 Simulation Results

Figure 1 illustrates the characteristics of all numerical simulations. Initially, C_A is uniform throughout the droplet volume, being equal to C^{eq}. As water begins to condense, C_A decreases at the surface layer, progressively diluting much of the droplet volume. This can be seen in Figure 2, which presents transient radial profiles of C_A. Simulations are shown for D_p = 1μm, D_c = 0.5μm, D_{Aw} = 1×10^{-10} m^2 s^{-1}, and s = 1%. The simulations

indicate that throughout most of the simulation, C_A drops steeply with distance from the core until a characteristic distance, R_s (Figure 1), after which the gradient of C_A becomes effectively zero (at steady state).

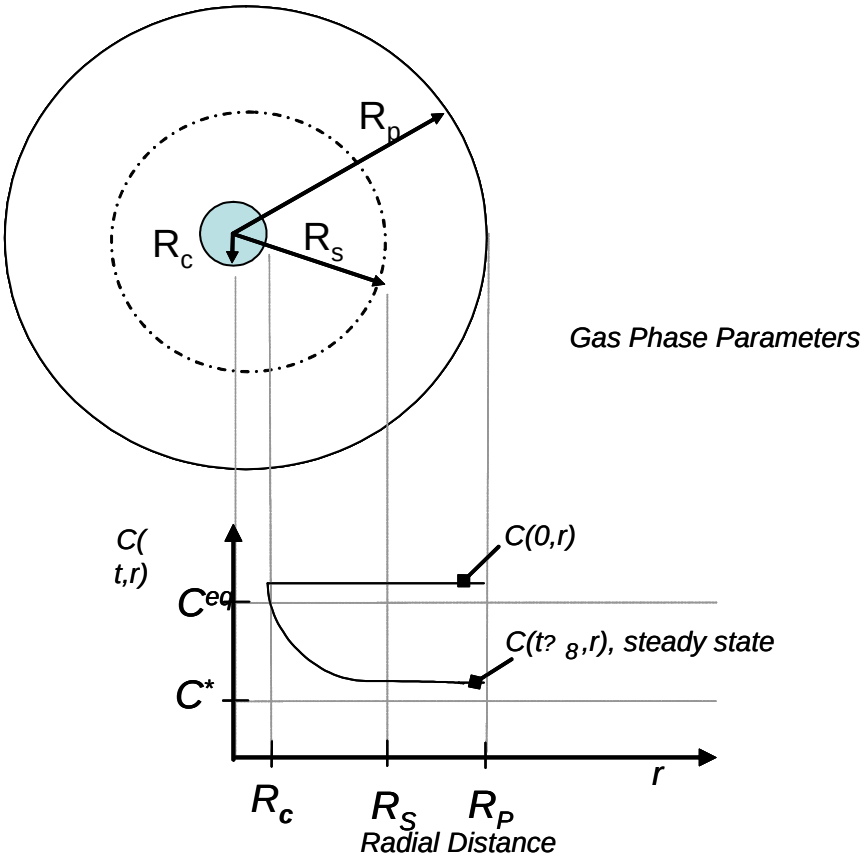

Figure 1: Illustration of the problem geometry and the solute concentration profile. R_s represents the location where the concentration gradient becomes effectively zero.

Figure 2 suggests that R_s may not significantly change location, and that the steady-state solution can be achieved in a fraction of a second, i.e. within the timescale of cloud droplet activation. It is therefore sufficient to focus on the steady-state concentration

profile, with an emphasis on the steady-state $C_A\left(t, R_p\right)$ (hereon referred to as C^*) because it determines the droplet equilibrium vapor pressure. Therefore, it is important to explore the dependence of the C^* on all four parameters varied in Table 1.

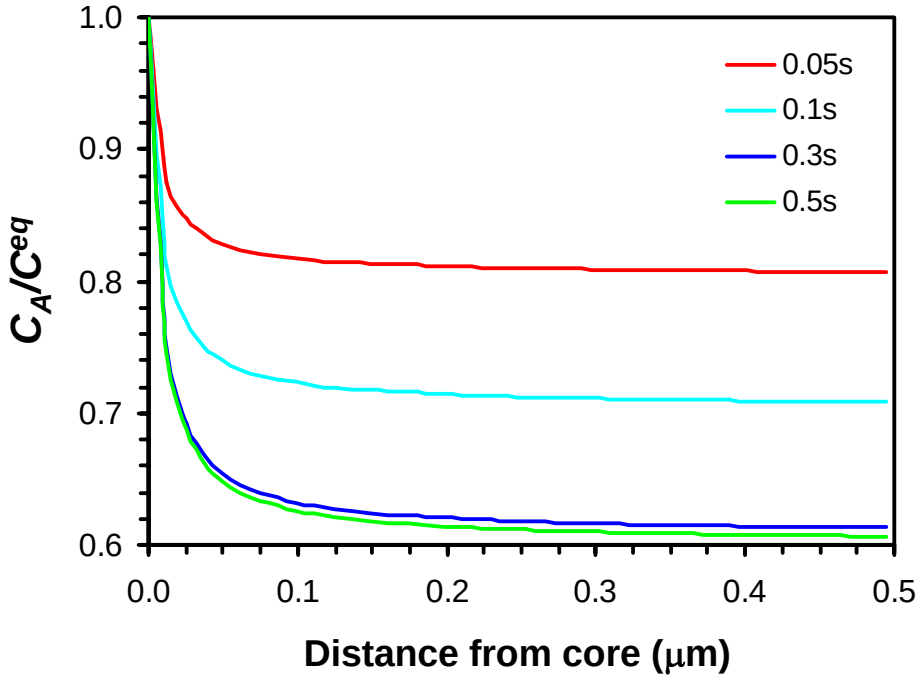

Figure 2: Transient radial profiles of C_A. Simulations are shown for D_p = 1μm, D_c = 0.5μm, D_{Aw} = 1×10^{-10} m^2 s^{-1}, and s = 1%.

Figure 3 presents steady-state radial profiles of C^*/C^{eq} for D_{Aw} ranging between 1×10^{-9} and 1×10^{-10} m^2 s^{-1}. Simulations are shown for D_p = 1μm, D_c = 0.5μm and s = 1%. As expected, the most pronounced decrease in C* occurs for the lowest molecular diffusivity (~10^{-10} m^2 s^{-1}), i.e., when mass transfer is the slowest. The simulations suggest

that the concentration depression is minor (~ 5%) for rapid mass transfer (D_{Aw} = 10^{-9} m^2 s^{-1}) but becomes significant (>10%) for D_{Aw} < 5×10^{-10} m^2 s^{-1}. The % depression in C^* seems to be inversely proportional to D_{Aw}.

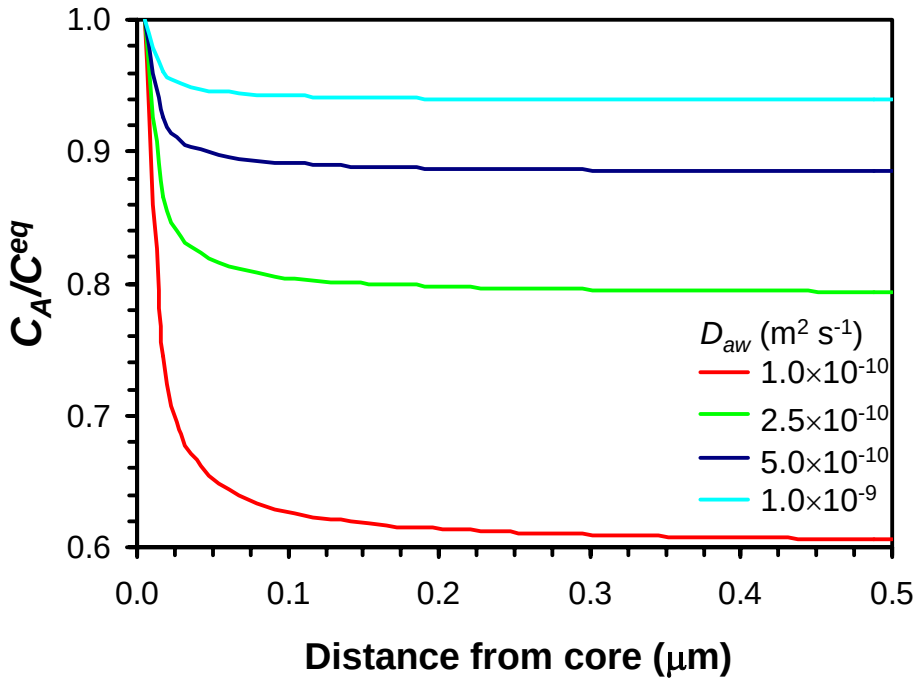

Figure 3: Steady-state radial profiles of C_A. Simulations are shown for D_p = 1μm, D_c = 0.5μm, s = 1%, and for D_{Aw} between 1×10^{-9} and 1×10^{-10} m^2 s^{-1}.

In addition to D_{Aw}, C^* depends on the droplet growth rate (i.e., the ambient supersaturation). This is depicted in Figure 4, which presents steady-state radial profiles of C^*/C^{eq} for s ranging between 0.1% and 1%. Simulations are shown for D_p = 1μm, D_c = 0.5μm, D_{Aw} = 1×10^{-9} m^2 s^{-1}. The largest drop in C^* is seen for high s, as this is the condition for which dilution of A from water condensation at the surface layer is strongest. Compared to D_{Aw}, an order of magnitude change in s leads to a smaller (but still significant) decrease in C^*.

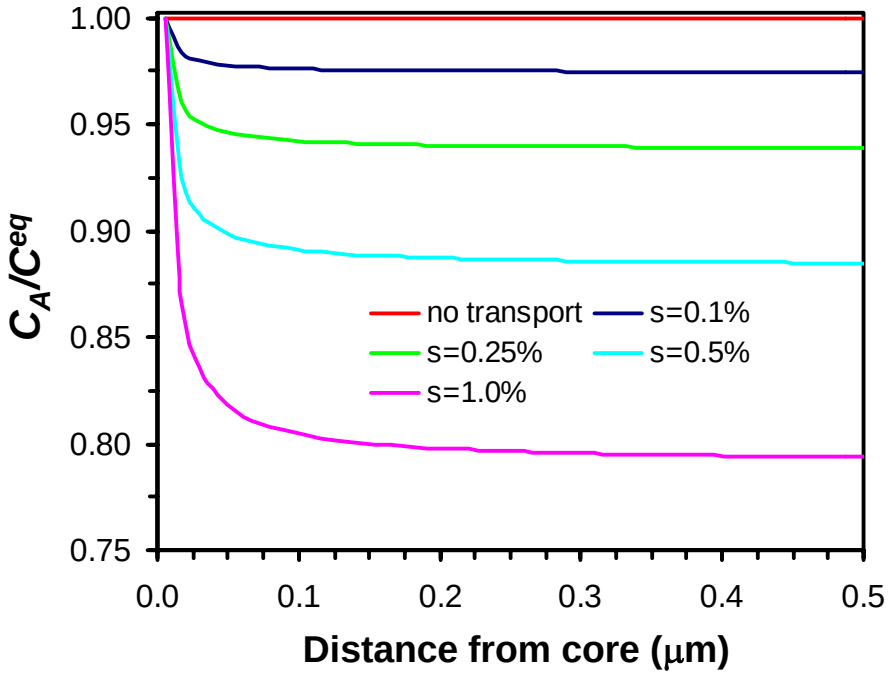

Figure 4: Steady-state radial profiles of C_A. Simulations are shown for D_p = 1μm, D_c = 0.5μm, D_{Aw} = 1×10^{-9} m^2 s^{-1}, and for s between 0.1% and 1%.

Finally, C^* depends on the droplet and core diameters. This is depicted in Figure 5, which shows C^*/C^{eq} as a function of core diameter and ambient supersatuation. Simulations are shown for (a) D_p = 1μm, D_{Aw} = 1×10^{-10} m^2 s^{-1}, and, (b) D_p = 5μm, D_{Aw} = 1×10^{-9} m^2 s^{-1}. It is clear that decreasing the core size and increasing the droplet size yield a larger depression in C^*, because mass transport becomes less efficient in supplying solute at the droplet surface. Simulations suggest that C^* can be fifty percent lower than C^{eq}.

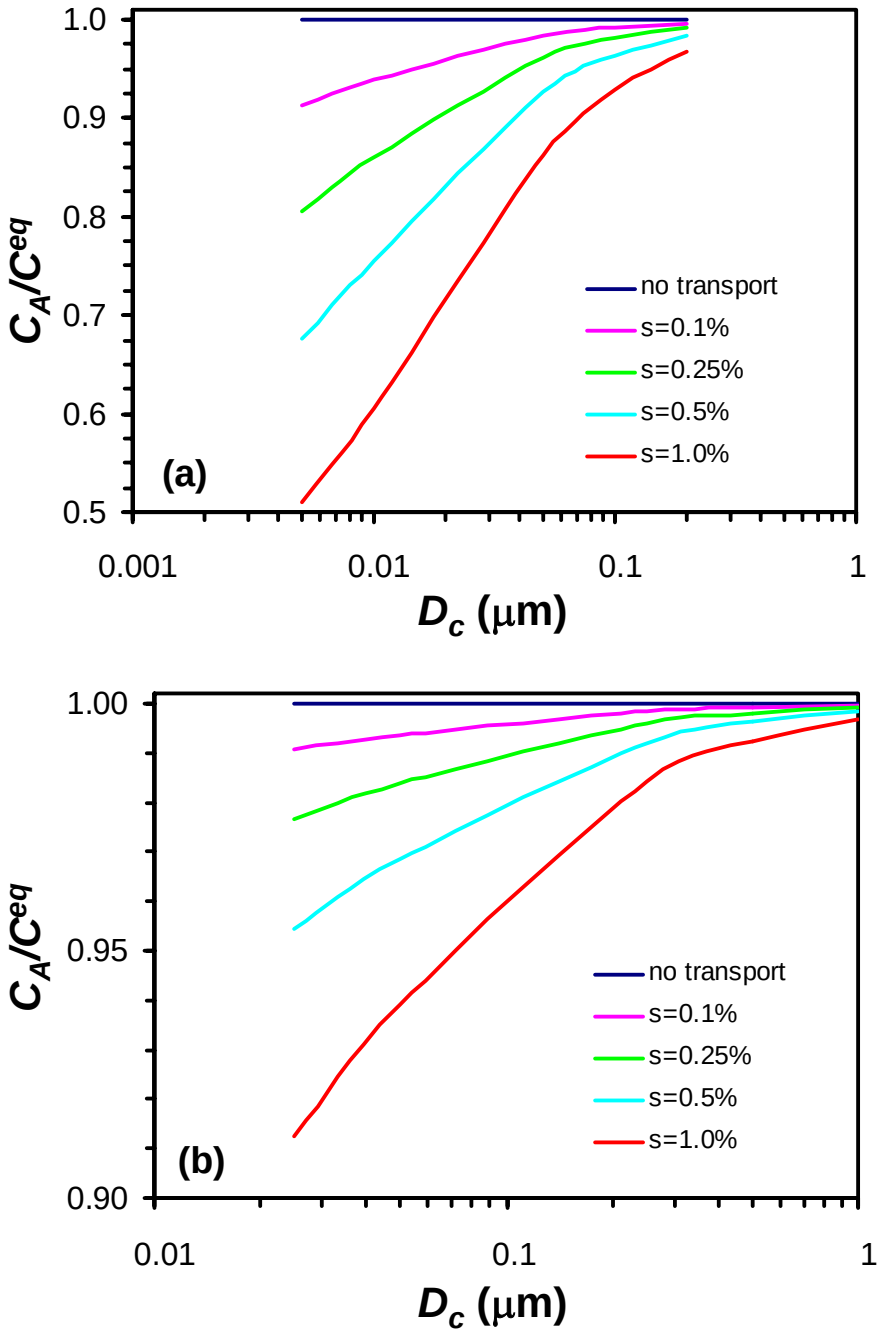

Figure 5: Steady-state droplet surface C_A normalized with Ceq, as a function of core diameter and ambient supersatuation. Simulations are shown for (a) D_p = 1μm, D_{Aw} = 1×10^{-10} m^2 s^{-1}, and, (b) D_p = 5μm, D_{Aw} = 1×10^{-9} m^2 s^{-1}.

The trends seen for C^* in the simulations can be rationalized through the following analysis. Applying the steady state requirement on the droplet surface boundary condition (Equation 10),

$$0 = -\frac{3}{D_p}\left[C_A(t,R_p)\left(\frac{dD_p}{dt}\right) + 4D_{Aw}\left(\frac{dC_A(t,R_p)}{dD_p}\right)\right] \tag{12}$$

$\left(\frac{dC_A(t,R_p)}{dD_p}\right)$ refers to the gradient of C_A at the droplet surface, and can be expressed as $\left(\frac{dC_A(t,R_p)}{dD_p}\right) \approx \frac{C^* - C^{eq}}{\Delta D_p}$, where ΔD_p is an appropriate spatial scale (more will be discussed in section 3.1). Substitution of the above into Equation (8) and solving for C^* yields,

$$C^* = \frac{C^{eq}}{\frac{\Delta D_p}{4 \cdot D_{Aw}}\left(\frac{dD_p}{dt}\right) + 1} \tag{13}$$

Substituting Equation (9) into (13) gives,

$$C^* = \frac{C^{eq}}{\frac{s}{4 \cdot D_{Aw} G}\left(\frac{\Delta D_p}{D_p}\right) + 1} \tag{14}$$

Equation 14 confirms the numerical simulation trends; when D_{Aw} is large, $C^* \approx C^{eq}$ and when it decreases, $C^* < C^{eq}$. Similarly, smaller droplet sizes or large ambient supersaturations will lead to large growth rates, and will decrease C^* because of excessive dilution of the surface layer. However, when the ambient supersaturation is very small or the droplet diameter is very large, $\frac{dD_p}{dt}$ is negligible and $C^* \approx C^{eq}$. D_c also affects C^*;

smaller sizes imply that the solute needs to diffuse over a larger distance, hence ΔD_p increases and C^* decreases.

3. INTRODUCING DISSOLUTION KINETICS INTO KÖHLER THEORY

3.1. Parameterization of the numerical simulations

It is desirable to introduce appropriate modifications to Köhler theory when assessing the effects of solute mass transfer kinetics on cloud droplet formation. This could be accomplished if a relationship is established between C^* and the dissolution kinetics parameters D_{Aw}, s, D_p and D_c. The steady-state droplet boundary condition (Equation 14) is ideally suited for this purpose; the free parameter ΔD_p however must first be defined. In deriving Equation (14), we assumed that $\left(\frac{dC_A(t,R_p)}{dD_p}\right) \approx \frac{C^*-C^{eq}}{\Delta D_p}$. Based on Figure 1, most of the variation of C_A takes place in a region close to the core; therefore the flux of A at the surface of the droplet can, at steady state, can be expressed as,

$$\left.\frac{dC_A(t,R_p)}{dD_p}\right|_{R_p} = \left.\frac{dC_A(t,R_p)}{dD_p}\right|_{Rs}\left(\frac{R_s^2}{R_p^2}\right) \approx \frac{C^*-C^{eq}}{R_s-R_c}\left(\frac{R_s^2}{R_p^2}\right) \tag{15}$$

where R_s is the distance where the concentration gradient becomes effectively zero (Figure 1). Defining $\omega = \frac{D_p}{D_c}$ and $\delta = 1-\frac{D_c}{D_s}$ (where D_s and D_p are diameters corresponding to R_s and R_p , respectively), Equation (15) becomes,

$$C^* = \frac{C^{eq}}{1+\delta(1-\delta)\frac{\omega s}{4GD_{Aw}}} \tag{16}$$

Equation (16) describes the solute surface concentration at the droplet surface in terms of solubility, ambient supersaturation, solute diffusivity, droplet and core size, and the non-dimensional coefficient δ which is related to the mass transfer kinetics. In agreement with the numerical simulations, Equation (16) indicates that a decrease in solute diffusivity and an increase ambient supersaturation both yield a decrease in the solute surface concentration. A small core size (i.e., increasing ω) implies that the solute has to diffuse a large distance; C^* will decrease because water vapor condensation is more efficient in diluting the droplet surface layer. We use the numerical simulations to constrain δ so that Equation (16) reproduces the steady-state C^* derived from the simulations. Least squares minimization yields $\delta = 0.933$ with which the numerical simulations are reproduced to within 10% (Figure 6).

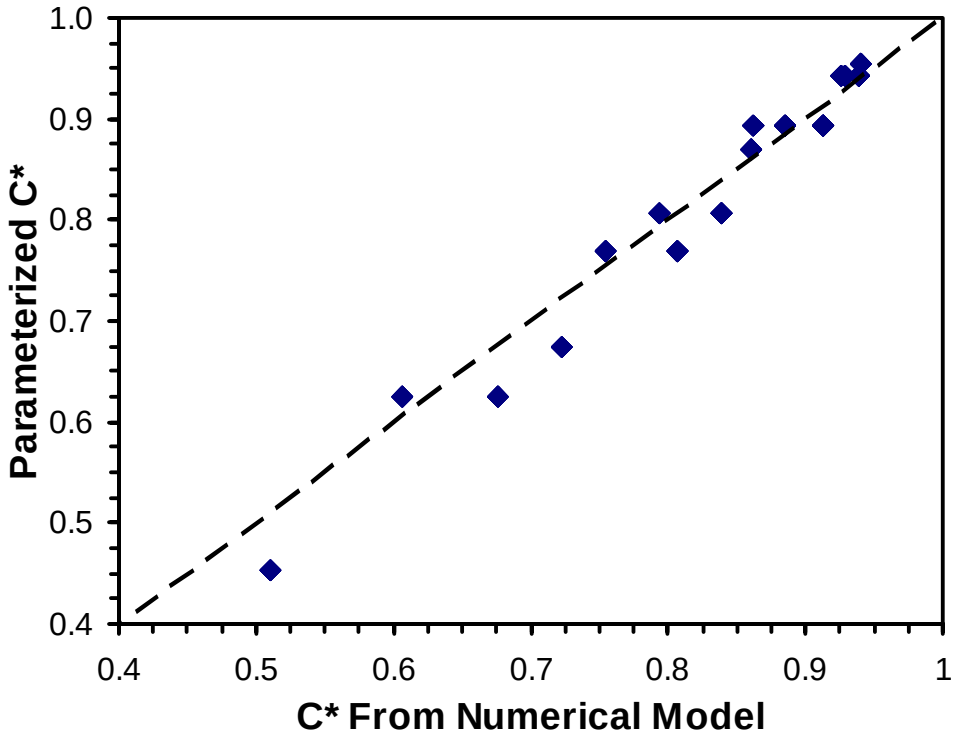

Figure 6: Parameterized vs. Simulation Surface Solute Concentration Values. Simulations are shown for which $C^* / C^{eq} \leq 0.95$.

An issue arises for small core diameters; as the core dissolves and approaches zero, $\omega \to \infty$; under such conditions, Equation (16) predicts that $C^* \to 0$. This is of course does not happen in reality but arises because Equation (16) was derived assuming steady-state for $C_A(t,r)$. When $D_c \to 0$, the steady state timescale becomes exceedingly long, and Equation (16) does not become applicable. This limitation is easily overcome by considering the droplet growth dynamics. Initially, droplet growth is at a rate that steady state assumptions can be made. The core begins to dissolve, shrink and eventually reaches a size in where Equation (16) is not applicable. At this instance, we will assume that C^* does not change anymore; thus a lower-limit constraint is applied on C^*. We

consider that a timescale relevant for cloud droplet formation is ~ 1 sec; under this constraint, numerical simulations suggest that $C^* \geq 0.5C^{eq}$. Therefore, the surface concentration of solute when mass transfer kinetics are considered is parameterized as,

$$C^* = \max\left\{0.5C^{eq},\ \frac{C^{eq}}{1+0.0625\frac{\omega s}{4GD_{AB}}}\right\} \tag{17}$$

3.2. Introduction to Köhler Theory

Solute mass transfer kinetics can be included in Köhler theory by appropriate modifications to existing theory. Assuming instantaneous dissolution for slightly solubles, the equilibrium supersaturation, s_{eq}, of a CCN composed of soluble (deliquescent) and a slightly soluble compounds can be expressed as (Shulman et al., 1996),

$$s_{eq} = \frac{4M_w\sigma_w}{RT\rho_w D_p} - \frac{6n_s M_w \upsilon_s}{\pi\rho_w D_p^{\ 3}} - \frac{6n_{ss} M_w \upsilon_{ss}}{\pi\rho_w D_p^{\ 3}} \tag{18}$$

where n_s, n_{ss} represents the moles of solute dissolved in the droplet from the soluble and slightly soluble species, respectively; $\upsilon_s, \upsilon_{ss}$ are the corresponding effective van't Hoff factors.

If the solubility of the partially soluble compound, C^{eq}, is expressed in moles m^{-3}, then in the presence of a soluble core (i.e., when there is not enough water in the CCN to completely dissolve the core) Equation (18) becomes,

$$s_{eq} = \frac{4M_w\sigma_w}{RT\rho_w D_p} - \frac{6n_s M_w \upsilon_s}{\pi\rho_w D_p^{\ 3}} - \frac{M_w}{\rho_w} C^{eq}\upsilon_{ss} \tag{19}$$

After the core has completely dissolved, Equation (18) is used with n_{ss} equal to the total moles of slightly soluble species available in the CCN.

Solute transport kinetics can be introduced in Equation (19) by replacing C^{eq} with C^{*} (Equation 17),

$$s_{eq} = \frac{4M_w\sigma_w}{RT\rho_w D_p} - \frac{6n_s M_w \upsilon_s}{\pi\rho_w D_p^{\,3}} - \frac{M_w}{\rho_w}\upsilon_{ss} \max\left\{0.5C^{eq},\ \frac{C^{eq}}{1+0.0625\dfrac{\omega s}{4GD_{AB}}}\right\} \tag{20}$$

We assume that after the core has completely dissolved, Equation (18) is used with n_{ss} equal to the total moles of slightly soluble species available in the CCN. This implies that mass transfer kinetics are not important after the core has dissolved; in reality there is a relaxation time associated with solute transport from the bulk of the droplet to the surface layer, which for simplicity we have neglected.

3.3. Implications of solute transport kinetics for cloud droplet formation

For solute dissolution kinetics to have an important influence on droplet formation: (a) a partially soluble core needs to be present during the CCN activation, and, (b) the amount of partially soluble solute provided is a significant fraction of the total solute. The latter requirement implies that solute dissolution kinetics may not influence droplet formation if the CCN contains substantial amounts of inorganic electrolytes (e.g., (NH4)2SO4). In the subsequent analysis, we consider CCN composed of only partially soluble substances so that the effects of dissolution kinetics on cloud droplet formation are maximized. In the atmosphere, such particles could correspond to aged secondary organic aerosol (VanReken et al., 2005).

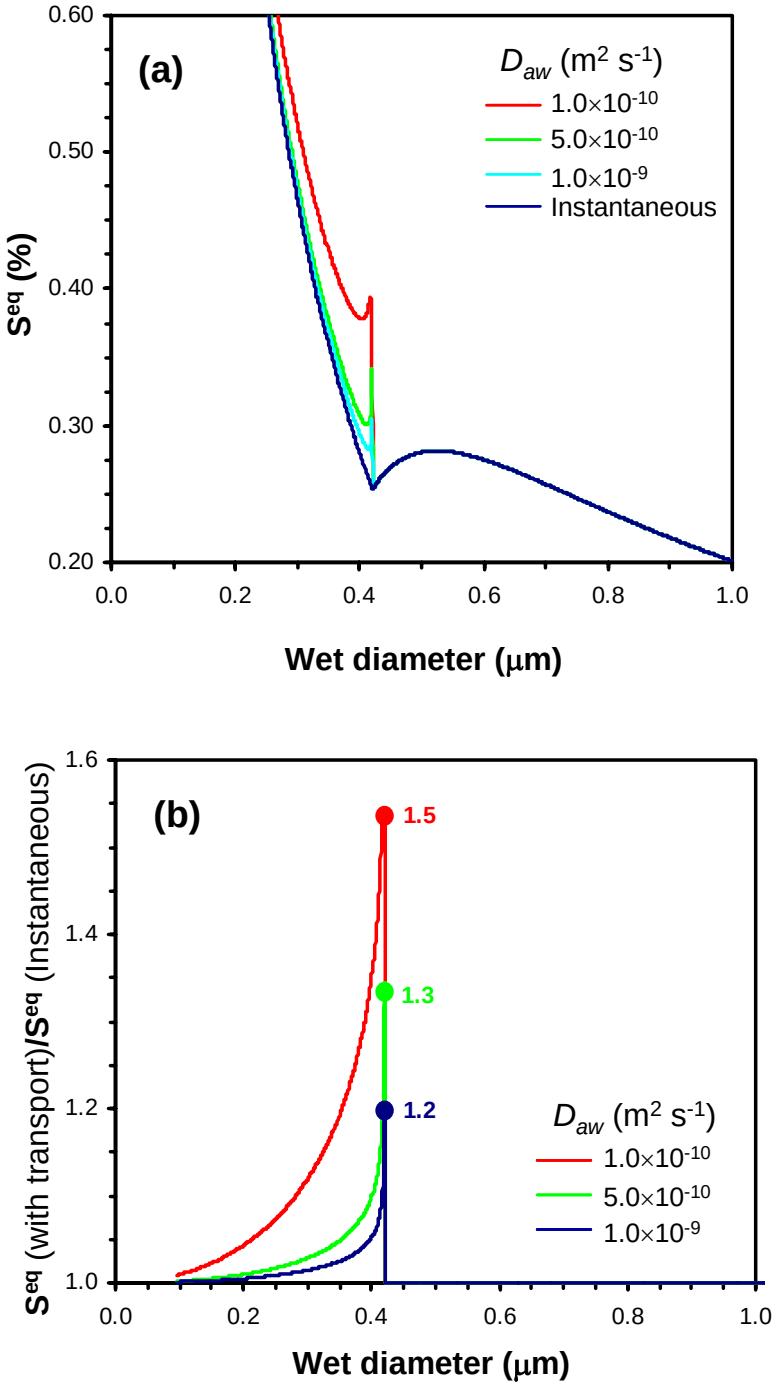

Figure 7: Köhler curves modified to include the effect of dissolution kinetics. The dry aerosol is 75 nm in diameter and composed of a partially soluble substance with 1750 kg m^{-3} density, 0.132 kg mol^{-1} molar mass, van't Hoff factor of 2 and a solubility of 10^{-2} kg kg^{-1}. Ambient supersaturation is assumed to be 1% . Calculations are presented as (a) S_{eq} vs. wet diameter for a range of D_{Aw}, and, (b) change in S_{eq}, relative to the instantaneous dissolution.

Figure 7 displays Köhler curves with and without the effect of solute dissolution kinetics. In these calculations, the dry CCN is 75 nm in diameter and composed of a partially soluble substance with 1750 kg m^{-3} density, 0.132 kg mol^{-1} molar mass, van't Hoff factor of 2 and a solubility of 10^{-2} kg kg^{-1}. Ambient supersaturation is assumed to be 1%. Assuming that dissolution and mass transfer of the solute is instantaneous (blue curves) yields "typical" Köhler curves (Figure 7a). At small wet diameters (< 0.4 μm), the amount of liquid water is insufficient to completely dissolve the core, hence the concentration of solute is constant throughout the droplet volume until complete dissolution (here at ~0.4 μm). For larger wet diameters, the droplet dilutes as it grows and develops the characteristic "Köhler" maximum in s_{eq}. When dissolution kinetics are considered, the decrease in C^* (Equation 17) shifts s_{eq} to higher levels at small wet diameters; this effect is rather small for large solute diffusivity (~ 10^{-9} m^2 s^{-1}) but becomes significant at modest to low diffusivity (~ 5×10^{-10} to 10^{-10} m^2 s^{-1}). This effect is more clearly seen if s_{eq} is normalized to s_{eq} from instantaneous dissolution (Figure 7b); the region where the ratio is larger than unity indicates an increase in equilibrium vapor pressure from the effect of dissolution kinetics. The effect of dissolution kinetics maximizes close to the point of complete dissolution of the core because the diffusion length scale (i.e., ω) becomes maximum. In Figure 7b, the increase in s_{eq} is at most 20% for large diffusivity (~ 10^{-9} m^2 s^{-1}), which is rather small. However, when the diffusivity is decrease, s_{eq} becomes significantly higher (~50%), exceeding the local maximum at ~0.5μm. The effects of dissolution kinetics become even stronger if a larger CCN is considered (not shown).

In addition to the diffusion coefficient and solubility, the droplet growth rate (i.e., ambient supersaturation) also affects s^{eq}. This is shown in Figure 8, which displays Köhler curves with the effect of solute dissolution kinetics for various ambient supersaturations. The CCN characteristics are the same as in Figure 7, and $D_{Aw} = 10^{-10}$ m s^{-2}. Calculations show that the Köhler curves exhibit rather important sensitivity to s (Figure 8a). As the ambient supersaturation drops and droplet growth slows down, dilution of the droplet surface layer from water condensation is less efficient, hence C^* approaches C^{eq} and s^{eq} converges to the "classical" Köhler (i.e., instantaneous transfer) curve. This effect is more clearly seen if s_{eq} is normalized to s_{eq} from instantaneous dissolution (Figure 8b); as in Figure 8b, dissolution kinetics maximizes close to the point of complete dissolution of the core.

Both Figures 7 and 8 imply that in the presence of solute dissolution kinetics, CCN could have a "dynamical" equilibrium saturation ratio that is considerably different from that obtained using only thermodynamic arguments. Although this may not be sufficient to completely inhibit CCN from becoming droplets, the modified droplet growth kinetics may have a strong influence on the water vapor availability during cloud droplet nucleation and feedback into cloud droplet number. For this, our newly developed theory needs to be incorporated into a numerical cloud parcel model (e.g., Nenes *et al.*, 2001); this will be the subject of a future study.

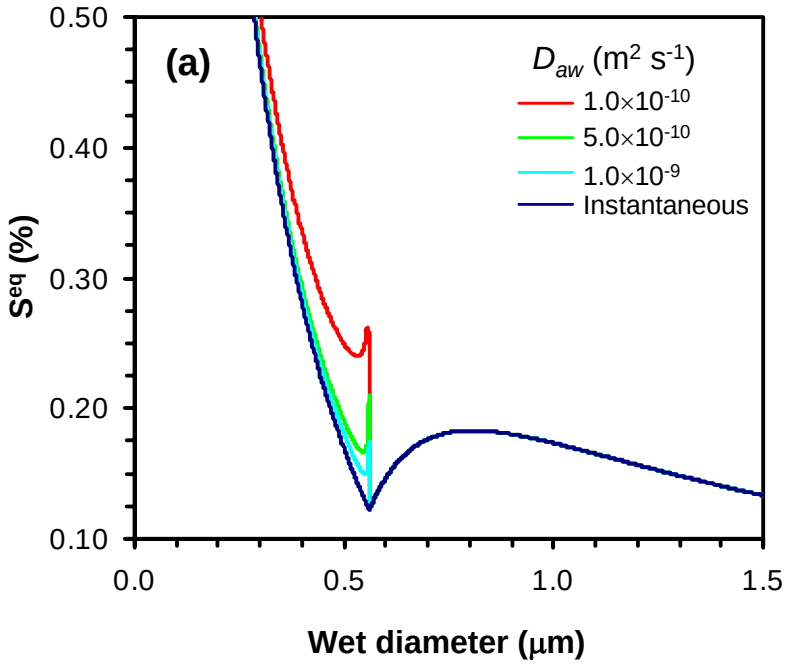

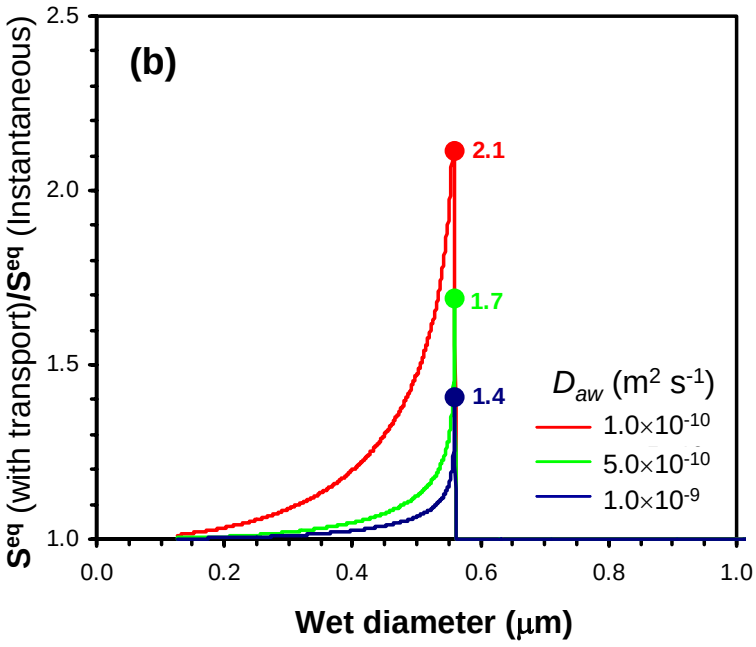

Figure 8: Same as Figure 7, but for a 100 nm dry particle diameter

CHAPTER 4: SUMMARY

Partially soluble substances, although able to affect the ability of cloud condensation nuclei (CCN) to form droplets, need a finite time to dissolve and diffuse to the droplet surface before they can affect droplet growth. This study focuses on the importance of dissolution kinetics for cloud droplet formation. To comprehensively account for the kinetics, a numerical model of the process was developed. Simulations of cloud droplet growth were performed for solute diffusivity, droplet growth rates, dry particle and droplet diameters relevant for ambient conditions. Simulations suggest that high ambient supersaturations and a decrease in solute diffusivity are major contributors to significant decreases in effective solute surface concentrations. Our simulations suggest that the effect of dissolution kinetics can lead up to a 50% decrease in surface solute concentration.

The steady-state numerical simulations were then parameterized and incorporated into Köhler theory to assess the impact of dissolution kinetics on the droplet equilibrium vapor pressure. For CCN composed of partially soluble material, a significant increase was found in the equilibrium supersaturation of CCN. Although this may not be sufficient to completely inhibit CCN from becoming droplets, the modified droplet growth kinetics may have a strong influence on the water vapor availability during cloud droplet nucleation and have a strong feedback on cloud droplet number. For this, our newly developed theory needs to be incorporated into a numerical cloud parcel model (e.g., Nenes *et al.*, 2001); this will be the subject of a future study.

REFERENCES

Blanchard, D. C. (1964). Sea-To-Air Transport Of Surface Active Material. Science 146(364): 396-&.

Chow, J. C., Watson, J. G., Fujita, E. M., Lu, Z. Q., Lawson, D. R. and Ashbaugh, L. L. (1994). Temporal and spatial variations of PM 2.5 and PM 10 aerosol in Southern California Air Quality. Atmospheric Environment 28: 2061-2080.

Chuang P. Y. (2003). Measurement of the timescale of hygroscopic growth for atmospheric aerosols. Journal of Geophysical Research 108 (D9): 4282.

Cruz, C. N. and S. N. Pandis (1997). A study of the ability of pure secondary organic aerosol to act as cloud condensation nuclei. Atmospheric Environment 31(15): 2205-2214.

Facchini, M. C., S. Fuzzi, S. Zappoli, A. Andracchio, A. Gelencser, G. Kiss, Z. Krivacsy, E. Meszaros, H. C. Hansson, T. Alsberg and Y. Zebuhr (1999). Partitioning of the organic aerosol component between fog droplets and interstitial air. Journal Of Geophysical Research-Atmospheres 104(D21): 26821-26832.

Facchini, M. C., M. Mircea, S. Fuzzi and R. J. Charlson (1999). Cloud albedo enhancement by surface-active organic solutes in growing droplets. Nature 401(6750): 257-259.

Feingold, G. and P. Y. Chuang (2002). Analysis of the Influence of Film-Forming Compounds on droplet Growth: Implications for Cloud Microphysical Processes and Climate. Journal of Atmospheric Science 59.

Gill, P. S., T. E. Graedel and C. J. Weschler (1983). Organic Films On Atmospheric Aerosol-Particles, Fog Droplets, Cloud Droplets, Raindrops, And Snowflakes. Reviews Of Geophysics 21(4): 903-920.

Hines, A. L. and R. N. Maddox (1985). Mass transfer: fundamentals and applications. Englewood Cliffs, N.J., Prentice-Hall.

IPCC (2001). Climate change: contribution of working group I to the third assessment report of the intergovernmental panel on climate change, Cambridge University Press.

Köhler, H. (1936). The nucleus in and the growth of hygroscopic droplets. Transactions of the Faraday Society 43: 1152.

Laaksonen, A., P. Korhonen, M. Kulmala and R. J. Charlson (1998). Modification of the Kuhler equation to include soluble trace gases and slightly soluble substances. Journal Of The Atmospheric Sciences 55(5): 853-862.

Lance, S., A. Nenes and T. A. Rissman (2004). Chemical and dynamical effects on cloud droplet number: Implications for estimates of the aerosol indirect effect. Journal Of Geophysical Research-Atmospheres 109(D22).

Limbeck, A., M. Kulmala and H. Puxbaum (2003). Secondary organic aerosol formation in the atmosphere via heterogeneous reaction of gaseous isoprene on acidic particles. Geophysical Research Letters 30(19).

Nenes, A., R. J. Charlson, M. C. Facchini, M. Kulmala, A. Laaksonen and J. H. Seinfeld (2002). Can chemical effects on cloud droplet number rival the first indirect effect? Geophysical Research Letters 29(17).

Nenes, A., S. Ghan, H. Abdul-Razzak, P. Y. Chuang and J. H. Seinfeld (2001). Kinetic limitations on cloud droplet formation and impact on cloud albedo. Tellus Series B-Chemical And Physical Meteorology 53(2): 133-149.

Novakov, T. and J. E. Penner (1993). Large Contribution Of Organic Aerosols To Cloud-Condensation-Nuclei Concentrations. Nature 365(6449): 823-826.

Perry, R. H., D. W. Green and J. O. Maloney (1997). Perry's Chemical Engineers' Handbook. New York, McGraw-Hill.

Pruppacher, H. and J. Klett (1997). Microphysics of Clouds and Precipitation. Norwell, Massachusetts, Kluwer Academy.

Raymond, T. R. and S. N. Pandis (2002). Cloud activation of single-component organic aerosol particles. Journal of Geophysical Research.

Seinfeld, J. H. and S. N. Pandis (1997). Atmospheric Chemistry & Physics: From Air Pollution to Climate Change, John Wiley & Sons.

Shantz, N. C., W. R. Leaitch and P. F. Caffrey (2003). Effect of organics of low solubility on the growth rate of cloud droplets. Journal Of Geophysical Research-Atmospheres 108(D5).

Shulman, M. L., M. C. Jacobson, R. J. Carlson, R. E. Synovec and T. E. Young (1996). Dissolution behavior and surface tension effects of organic compounds in nucleating cloud droplets. Geophysical Research Letters 23(3): 277-280.

Sloane, C. S., Watson, J., Chow, J., Pritchett, L. and Richards, L.W. (1991). Size-segregated fine particle measurements by chemical species and their impact on visibility impairment in Denver. Atmospheric Environment 25A: 1013-1024.

VanReken, T., Rissman, TA, Roberts, GC, et al. (2003). Toward aerosol/cloud condensation nuclei (CCN) closure during CRYSTAL-FACE. Journal of Geophysical Research - Atmospheres 108 (D20).

VanReken, T. M., N. L. Ng, R. C. Flagan and J. H. Seinfeld (2005). Cloud condensation nucleus activation properties of biogenic secondary organic aerosol. Journal Of Geophysical Research-Atmospheres 110(D7).

Wolff, G. T., Ruthosky, M. S., Stroup, D. P. and Korsog, P. E. (1991). A characterization of the principal PM-10 Species in Claremont (summer) and Long Beach (Fall) during SCAQS. Atmospheric Environment 25A: 2173-2186.